

# Long-term geoelectrical monitoring of landslides in natural and engineered slopes

Jonathan Chambers<sup>1</sup>, Jessica Holmes<sup>2</sup>, Jim Whiteley<sup>1</sup>, James Boyd<sup>1,3</sup>, Philip Meldrum<sup>1</sup>, Paul Wilkinson<sup>1</sup>, Oliver Kuras<sup>1</sup>, Russell Swift<sup>1,4</sup>, Harry Harrison<sup>1</sup>, Stephanie Glendinning<sup>2</sup>, Ross Stirling<sup>2</sup>, David Huntley<sup>5</sup>, Nick Slater<sup>6</sup>, and Shane Donohue<sup>7</sup>

<https://doi.org/10.1190/tle41110768.1>

## Abstract

Developments in time-lapse electrical resistivity tomography (ERT) technology are transforming our ability to monitor the subsurface due to purpose-built monitoring instruments, advances in automation and modeling, and the resulting improvements in spatial and temporal resolution. We describe the development of a novel ERT-based remote monitoring system called PRIME that integrates new low-power measurement instrumentation with data delivery, automated data processing and image generation, and web-based information delivery. Due to the sensitivity of ERT to hydrologic processes in the near surface, we focus on the application of PRIME for moisture-driven landslide monitoring. Case examples are considered of landslides in engineered and natural slopes, including those impacting geotechnical assets in rail and highways, where slope hydrology is seen to be controlled by lithology, vegetation, fissuring, and drainage structures. We conclude by taking a forward look at emerging developments in ERT monitoring relating to hardware, software and modeling, and applications.

## Introduction

Recent years have seen an increasing focus on the role of geophysics for monitoring landslides and slopes that are vulnerable to instability (e.g., Whiteley et al., 2019). This has been driven not only by developments in geophysical instrumentation and modeling tools but also by parallel advances in landslide early-warning science (Intrieri et al., 2013; Whiteley et al., 2021) and in the remote condition monitoring of engineered slopes by the civil engineering community (Smethurst et al., 2017).

Electrical resistivity tomography (ERT), or resistivity imaging, is perhaps the most widely used geophysical method for characterizing and monitoring natural and engineered slopes at risk of failure (Whiteley et al., 2019; Fan et al., 2021; Dimech et al., 2022). Resistivity is sensitive to compositional variations and, most importantly for landslide monitoring, moisture-driven changes (Lapenna and Perrone, 2022). Furthermore, ERT technology is readily configurable for monitoring applications (Slater and Binley, 2021). A single system can address potentially hundreds of low-cost electrodes (or sensors), and active measurements can be made from

battery-powered instruments (as compared to most other geophysical approaches for which sensor costs are currently prohibitive for long-term geophysical imaging or require mobile and/or high-energy sources). Initially, ERT monitoring has been achieved through adapting existing survey instruments for long-term monitoring applications, although these systems are generally expensive, designed for higher-power applications (e.g., greater than 200 W for deeper exploration), and often with limited communications and control functionality (e.g., embedded controllers, telemetry, and diagnostics). In particular, power consumption is a key challenge for high-power conventional ERT instruments that require mains electricity supply for battery recharge (which rules out monitoring in remote locations) or large solar arrays or fuel cells (which drives up the cost and complexity of the installation). The development of low-power instruments (e.g., 10 W) and bespoke monitoring systems (e.g., Tresoldi et al., 2019; Holmes et al., 2020) with telemetric control is enabling increasingly widespread use of resistivity monitoring (Whiteley et al., 2019). In addition to hardware developments for long-term ERT monitoring, it has long been recognized (e.g., LaBreque et al., 2004; Versteeg et al., 2004) that software developments are required for automated data management and processing. This is because, for large time-series data sets from multiple field sites, manual processing is impractical, and near-real-time information delivery is impossible.

Here, we consider a novel purpose-built ERT monitoring system — referred to here as the PRIME (proactive infrastructure monitoring and evaluation) system — designed to address the aforementioned technological challenges. The system concept and components are described, and the application of the system to landslide monitoring is considered through a series of case histories on natural and engineered slopes.

## PRIME technology overview

The PRIME system concept is shown in Figure 1. It comprises four essential elements: (1) field measurement; (2) control and data storage; (3) data processing and interpretation; (4) and decision support.

**Field measurement.** The PRIME hardware, designed and built by the British Geological Survey, consists of a low-power

<sup>1</sup>British Geological Survey, Nottingham, UK. E-mail: jecha@bgs.ac.uk; jwhi@bgs.ac.uk; jamyd91@bgs.ac.uk; pime@bgs.ac.uk; pbw@bgs.ac.uk; oku@bgs.ac.uk; russells@bgs.ac.uk; hharr@bgs.ac.uk.

<sup>2</sup>Newcastle University, Newcastle upon Tyne, UK. E-mail: jessica.holmes@newcastle.ac.uk; stephanie.glendinning@newcastle.ac.uk; ross.stirling@newcastle.ac.uk.

<sup>3</sup>Lancaster University, Lancaster, UK.

<sup>4</sup>University of Liège, Liège, Belgium.

<sup>5</sup>Geological Survey of Canada, Vancouver, British Columbia, Canada. E-mail: david.huntley@nrcan-rcan.gc.ca.

<sup>6</sup>Socotec Monitoring Ltd., East Sussex, UK. E-mail: nick.slater@socotec.com.

<sup>7</sup>University College Dublin, Dublin, Ireland. E-mail: shane.donohue@ucd.ie.

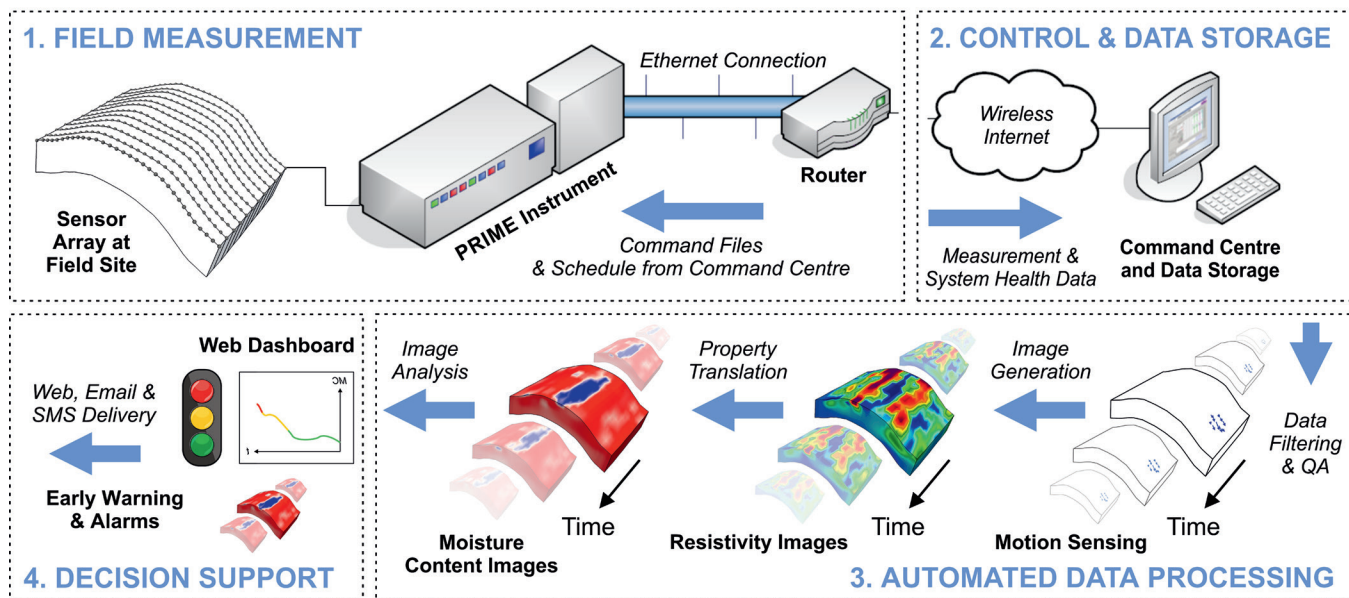


Figure 1. PRIME system concept (adapted from Holmes et al., 2020).

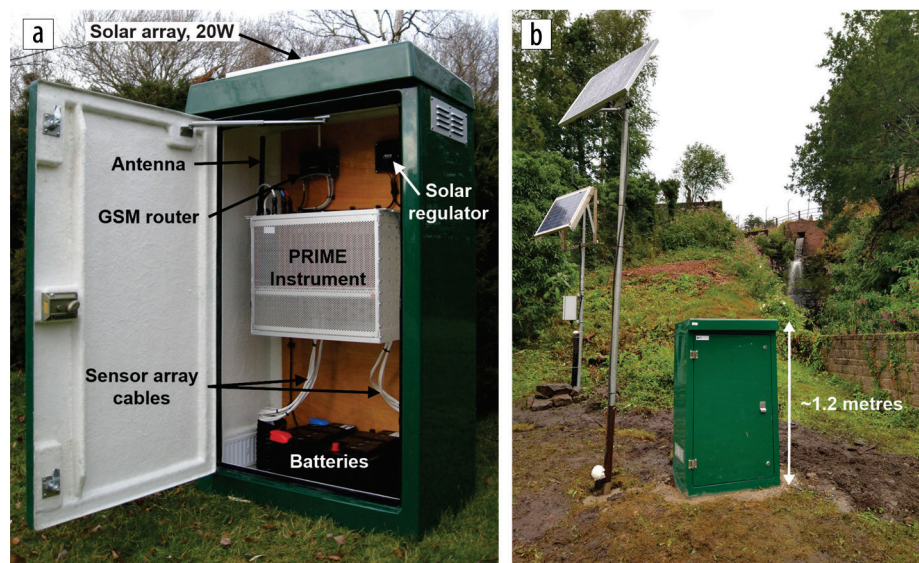


Figure 2. PRIME installation showing (a) system components and (b) enclosure and solar panel.

(10 W) resistivity meter, 4G/5G router, solar regulator, and batteries. The instrument is typically housed in a small enclosure, with a footprint of 40 × 70 cm (Figure 2). It is designed to address up to 512 electrodes and has seven channels for simultaneous measurements. It is constructed using a modular design with a plug-and-play main controller board and electrode address cards. Each element can be readily replaced in the field, enabling easy servicing and maintenance. It has local data storage for up to 100 measurement files and 50 command files (specifying electrode selection, current, measurement frequency, and number of cycles). The PRIME system can also address point sensors (e.g., soil moisture, rain gauge, etc.). These point sensors can automatically trigger periods of higher-frequency measurement, e.g., in response to an extreme rainfall event that exceeds a threshold at which a critical state may be reached. Such thresholds

can be established by studying previous failure states in similar and/or nearby sites, or they can be inferred from the PRIME system once long-term monitoring baselines have been established (e.g., Uhlemann et al., 2017). Once the field system is configured, its operation is fully automatic. The number and spacing of electrodes and the selection of acquisition array type are determined by the project's requirements (see case histories).

**Control and data management.** The command center (accessible through any networked phone, tablet, or PC) is used to remotely address and configure PRIME instruments. A web interface is used to specify command files and measurement schedule. Once a measurement set is made, it is automatically

transferred back to the command center for storage before data processing. Along with ERT and point sensor measurements, the command center also retrieves system health data (i.e., charge current, battery levels, electrode contact resistances, and measurement errors) (Figure 3). Summary health information is automatically e-mailed to predefined mailboxes for operator assessment.

**Data processing and interpretation.** The data processing and interpretation workflow has been designed as a series of linked modules. The first step is to scan for incoming data, combine relevant data files, and generate quality assurance and descriptive statistics. For unstable slopes where electrode displacements can be anticipated, a module has been developed to estimate electrode displacements from the electrical data (Wilkinson et al., 2016) to track slope movement and update electrode positions prior to inversion. Time-lapse sequences are then assembled and images

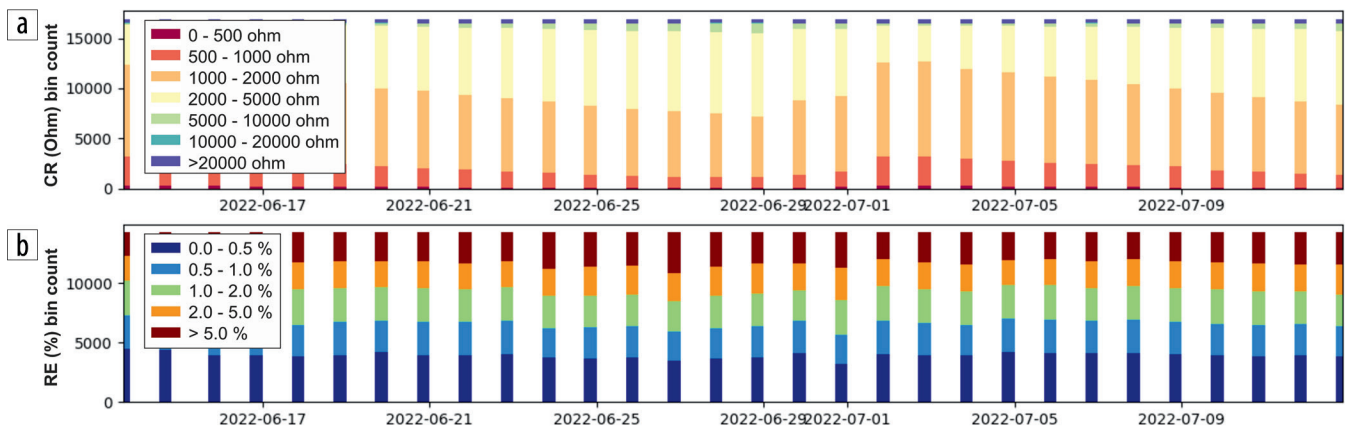


Figure 3. Example of an automatically generated PRIME system health plot showing (a) average contact resistance and (b) reciprocal error statistics.

generated (inversion). The workflow is designed to be flexible and has the potential to accommodate different forward modeling and inversion codes. Currently, the system is configured for using RES3DINV (Loke et al., 2014). Once the resistivity images have been generated, corrections can be applied to remove the effects of seasonal ground temperature variations on resistivity measurements. Furthermore, laboratory-derived relationships between resistivity and other key material properties can be applied — for example, to estimate spatial variation in gravimetric moisture content (GMC) from the resistivity images (Holmes et al., 2022a).

**Decision support.** A key focus of PRIME development has been to make ERT monitoring information available and intelligible to end users. This has been achieved by integrating ERT imaging results into a pre-existing geotechnical web dashboard (Calyx-OMS). Key advantages of this approach include the integrated display and analysis of geotechnical and geophysical information, and incorporation of geophysical monitoring data into a standardized geotechnical delivery environment. The dashboard is designed to ingest data from geotechnical point sensors (e.g., tilt, moisture content, pore pressure, etc.) for near-real-time display and interrogation. Alarm states can be defined for each sensor, with notifications sent to operators through e-mail or SMS (text messages). PRIME outputs have now been integrated into this information delivery environment, so each cell or pixel of the resistivity image is treated as an individual point sensor. The environment includes a 4D visualization window allowing the user to interact with the monitoring results through rotating, slicing, and defining iso-volumes in images. Likewise, alarm thresholds can be set for individual cells/voxels or for regions of the images.

## Case histories

**Old Dalby, UK — Stabilized landslide in a rail cutting.** ERT monitoring was undertaken over two years (July 2015–July 2017) on a relict landslide on the Old Dalby railway cutting, adjacent to the Old Dalby test track in Leicestershire, UK. The Old Dalby railway cutting has a history of instability, which is typical for significant elements of the transport network in the United Kingdom, owing to aging assets that were constructed during the industrial revolution (Gunn et al., 2016). The spatial

variation in vegetation across the monitored area of the slope at the cutting provides an opportunity to assess the influence of vegetation type on slope stability (Holmes et al., 2022b); indeed, a relict landslide in the center of the monitored zone is characterized by grasses and mosses, and on either side of this, the railway cutting is wooded with broadleaf deciduous trees (predominantly hawthorn).

The PRIME installation at Old Dalby consisted of buried, stainless steel rod electrodes set out in five lines: two running across slope and three running downslope, extending across a relict landslide and sections of unslipped cutting on either side. Electrode arrays running across slope consisted of 91 electrodes at 1 m spacing, and electrode arrays running downslope consisted of 19 electrodes at 1 m spacing. The system was powered using a 100 W solar panel, making it independent from mains power supply. Measurement sets were acquired automatically once every 12 hours using a dipole–dipole array configuration.

A baseline image (Figure 4a) shows the location of the PRIME arrays in relation to the wooded and grassed parts of the cutting. Figure 4b shows average resistivity through time for the grassed and wooded areas of the monitored section of the slope at the cutting as well as average resistivity for the slope as a whole. Weather data are also shown to aid interpretation of the resistivity data with respect to changes in resistivity and GMC through time. The GMC is estimated through laboratory testing to determine a site-specific relationship between resistivity and moisture content (Holmes et al., 2022b).

Seasonal changes in resistivity (and in GMC) are observed in the wooded regions of the slope and are closely related to changes in weather conditions. Low GMC in summer (maximum average resistivity of 50.9  $\Omega\text{m}$ ) in the wooded areas of the slope corresponds to negative effective rainfall. In winter, when positive effective rainfall is prevalent, GMC is high (minimum average resistivity of 26.0  $\Omega\text{m}$ ). However, these seasonal changes were not observed in the grassed region of the slope (resistivity ranged between 20.4 and 25.3  $\Omega\text{m}$ ), where changes in resistivity and GMC were smaller. The spatial differences in resistivity (and therefore in GMC) across the Old Dalby railway cutting are attributed to the variations in vegetation type: tree activity is higher in summer than in winter, as increased daylight and

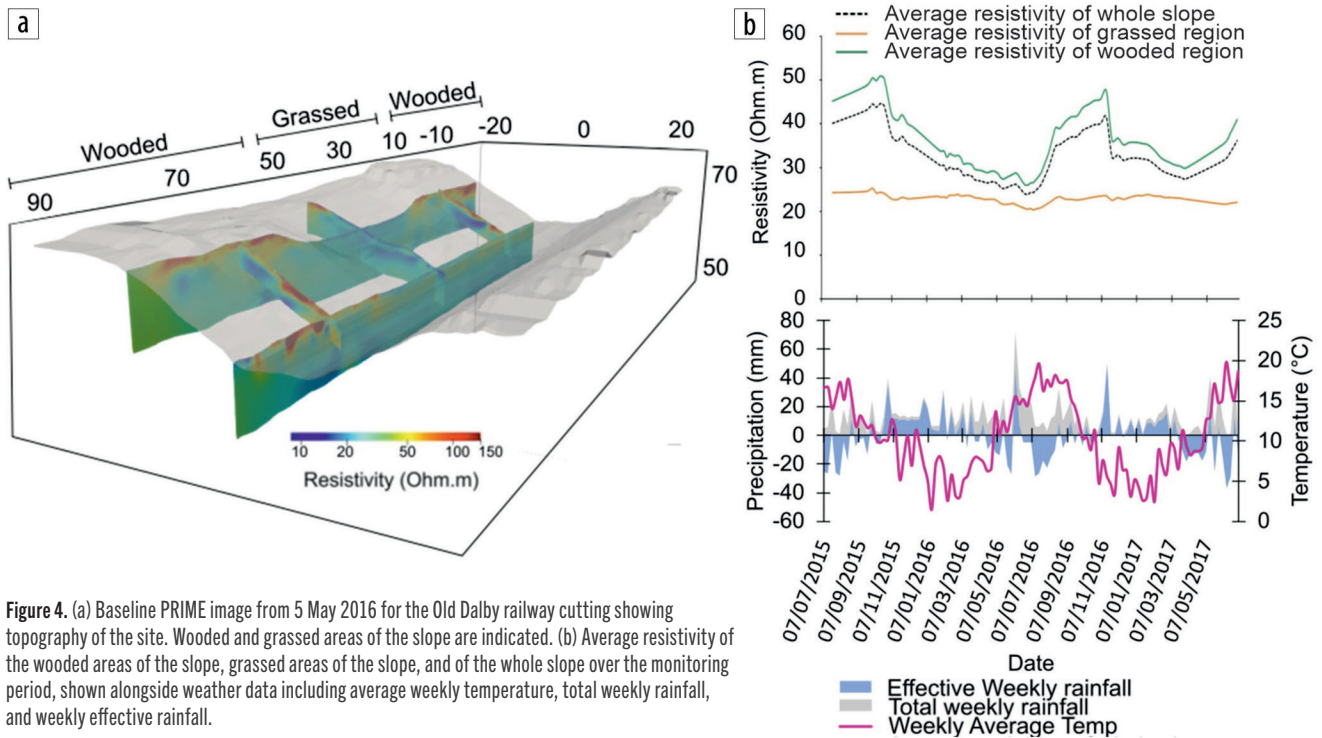


**Figure 4.** (a) Baseline PRIME image from 5 May 2016 for the Old Dalby railway cutting showing topography of the site. Wooded and grassed areas of the slope are indicated. (b) Average resistivity of the wooded areas of the slope, grassed areas of the slope, and of the whole slope over the monitoring period, shown alongside weather data including average weekly temperature, total weekly rainfall, and weekly effective rainfall.

increased temperatures result in higher rates of photosynthesis that lead to increased transpiration and root water uptake (Vivoni et al., 2008). In winter, this plant activity is reduced, and rainfall interception and canopy storage are reduced due to leaf loss, which explains the reduction in the difference in resistivity between wooded and grassed areas during this time.

As such, vegetation type is important for slope stability, owing to the controls on soil moisture and matric suction generation. For example, shrink-swell behavior is more likely in wooded areas due to an increase in the magnitude of wetting and drying on a seasonal basis when compared with grassed areas. This can reduce shear strength of the soil and result in deformation and slope failure (Khan et al., 2019). However, high soil-moisture levels (as indicated by the low resistivities recorded in this region of the slope), associated with grassed areas, also increase susceptibility to failure, owing to increases in pore water pressure. This highlights the utility of ERT monitoring for cut slopes, as it enables insight into key factors affecting slope stability in this setting.

**Hollin Hill, UK — Active rural landslide.** The Hollin Hill landslide observatory was established by the British Geological Survey in 2008. Since that time, near-continuous geoelectrical monitoring has been undertaken, initially using automated time-lapse ERT (Uhlemann et al., 2017) and more recently, since October 2020, using the more power-efficient and cost-effective PRIME system. Alongside geophysical monitoring, the field site has been instrumented with various sensors that are sensitive to ground movements, temperature, and local weather (e.g., Kelevitz et al., 2022). The observatory is situated on a 12° south-facing slope of Lower Jurassic sedimentary rocks located in the Howardian Hills in the northeast of England. The geology of the landslide broadly consists of two major formations, the Whitby Mudstone Formation (WMF), which conformably lies on the

Staithe Sandstone Formation (SSF). The WMF is widely regarded as an unstable geologic unit that spans much of England and is responsible for many landslides (Hobbs et al., 2005). In this case, geoelectrical monitoring is employed to monitor the moisture content of an active landslide.

The array setup at Hollin Hill consists of seven electrode lines, each with 32 electrodes spaced at a 4.5 m interval (Figure 5a). The setup of the electrode arrays is such that the system spans the length of the hillside (from head to toe of the sliding material), covering an area actively undergoing rotational failure and flow lobes. Dipole-dipole measurement sets along and across electrode arrays are completed once every 24 hours, including the collection of reciprocal data sets. The system is powered by a solar array.

Petrophysical relationships developed for the Whitby Mudstone allow for the conversion of resistivity into moisture content after a seasonal temperature correction. Therefore, PRIME can be used to monitor volumetric changes in moisture content in this case. The landslide has moved several times during monitoring, with major episodes in 2012 and 2016 during periods of elevated moisture contents (or relatively low resistivities). During the PRIME monitoring period, further movements have been observed within earthflow in the lower regions of the slope (Figure 5a), while the rotational back scarp feature, which developed in 2016, has continued to migrate west.

In the baseline ERT image, the two dominant lithologies present at Hollin Hill can be identified (Figure 5b). The lower resistivities observed (less than 30 Ωm) correspond to the WMF present toward the top of the slope. Higher resistivities at Hollin Hill correspond to the SSF (greater than 30 Ωm). Additionally, in the baseline image, the outline of the flow lobes at Hollin Hill can be observed. These are a low-resistivity region on the SSF. Time-lapse processing of the PRIME data shows low GMC

during the summer months, corresponding to the largest resistivities observed at the site (Figure 5d), while the lowest resistivities are observed during the winter months (Figure 5c). This shows that the PRIME system is sensitive to seasonal changes in moisture content. In January 2021, movement was recorded by a grid of surface marker pegs. These movements were observed in front of the rotational back scarp toward the top of the slope (Figure 5a) and inside the flow lobes (Figures 5a–5c), which suggests elevated moisture contents in these parts of the slope have encouraged further movement. To conclude, the PRIME system illuminates hydrologic conditions occurring at the time of landslide movements, providing the basis for integrating PRIME into a landslide early-warning or modeling framework.

**Leys Bend, UK — Dormant landslide in a natural slope impacting highway infrastructure.** The A40 dual carriageway is a major strategic road linking England and Wales. A PRIME system was deployed between July 2017 and February 2019 on a section of potentially unstable slope immediately above the A40 at Leys Bend. The slope on this section of road, located approximately 2.5 km northeast of Monmouth, Wales, predominantly consists of sandstones interbedded with subordinate mudstone. The angle of dip in these beds, broadly aligned with the slope angle (approximately 30°), and the presence and thickness of the weaker mudstone bands makes the slope susceptible to failure. The A40 was affected by landslide activity during construction between 1964 and 1965. One landslide, the Whipping Green landslide, induced gradual but significant subsidence of the inter-carriageway embankment. A second landslide, the Chapel Farm landslide, experienced gradual displacements over several months before accelerating to total failure after a period of heavy rainfall, destroying both carriageways and several farm buildings located at the base of the slope (Early and Jordan, 1985).

During the redesign of the carriageway and installation of engineered mitigation measures, an area of ground showing initiation of displacement was observed above the carriageway. Based on measurements from recent LiDAR scans and field estimates of depth to the sliding surface, this “partially slipped area” (PSA) has an approximate volume between  $2.7$  and  $6.75 \times 10^4 \text{ m}^3$ , with the toe of the area terminating only 20 m above the existing carriageway. Since completion of the A40 in 1968, monitoring through to 2005 found no further displacement (Smedley et al., 2009), and a comparison of LiDAR data between 2006 and 2020 confirms that no widespread movement has occurred recently. Nonetheless, the presence of a large unstable mass above a

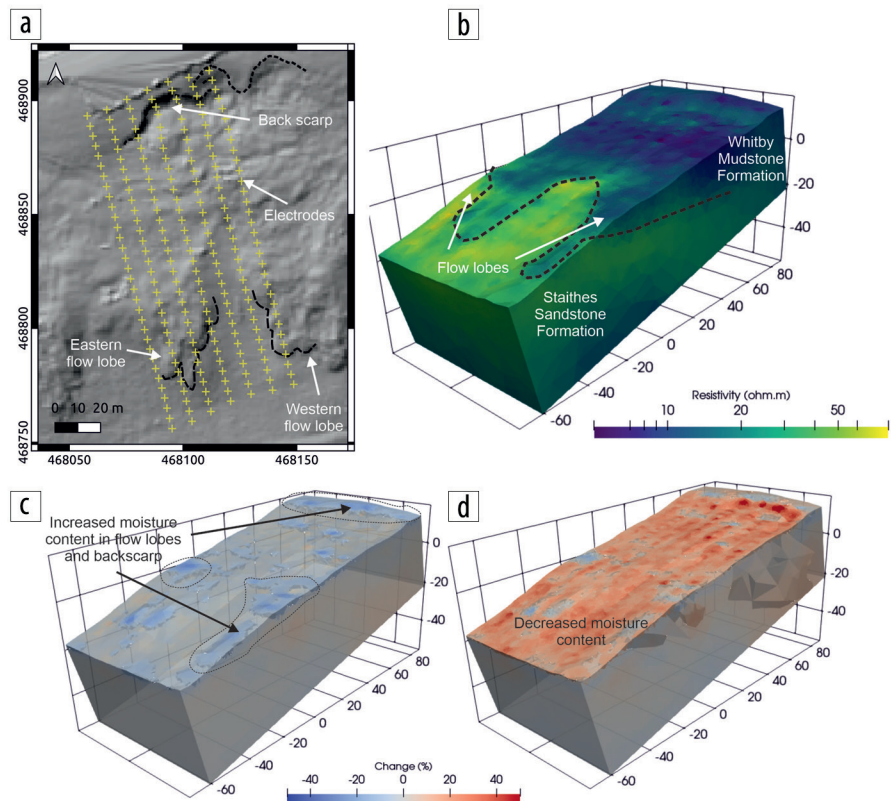


**Figure 5.** (a) Overview of the Hollin Hill landslide, showing a hillshaded base map, electrode positions as of October 2020, back scarp, and flow lobes. (b) Baseline resistivity inversion image showing the geology of the slope. (c) Time-lapse inversion image for 20 January 2021 showing changes in resistivity. (d) Time-lapse inversion image for 9 May 2021, again presented as a percentage change.

strategically significant highway in an area of historic landslide activity still poses a significant, if not immediate, risk to the A40 dual carriageway.

The PRIME system was deployed to monitor rainfall-driven hydrogeological changes in the subsurface of the PSA. The system comprised two linear arrays of 64 electrodes each, with a nominal 2 m separation between electrodes. One array was deployed parallel to the direction of slope (the “upslope” line) and situated entirely within the PSA; the other array was deployed perpendicular to slope angle (the “cross” line) and was situated partially within the PSA and partially in stable ground (Figure 6a). Measurements were acquired using a dipole-dipole array configuration. The system was deployed to the slope in July 2017. A baseline data set was acquired on 21 July 2017 from which relative changes in resistivity were determined. The result of the monitoring clearly demonstrates the differential infiltration patterns created by the formation of a “slip mosaic” within the sandstone layers in the PSA. This mosaic is characterized by vertical jointing in the sandstone as the strata accommodate the minor displacements of the PSA, with joint separations ranging from one to tens of meters. These joints create preferential pathways for water infiltration, allowing water to infiltrate to greater depths within the PSA, and showing areas of decreased resistivity relative to the baseline (blue zones) within the subsurface of the PSA. Areas of increased resistivity in the near surface are indicative of larger intact blocks of sandstone with wider joint separations and lower volumes and

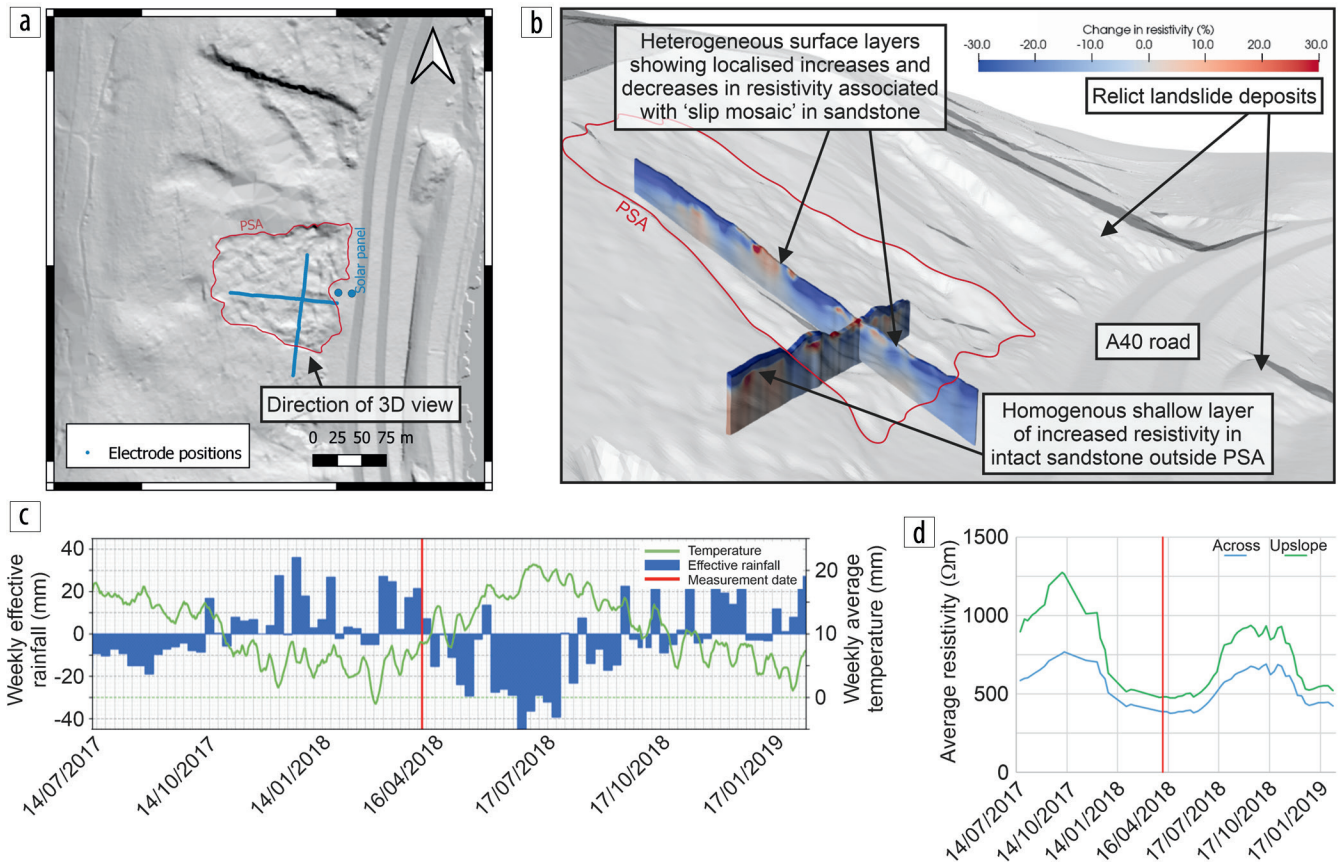


**Figure 6.** (a) Plan view of the PRIME system situated on the PSA, located above the A40 dual carriageway. (b) Three-dimensional view of the PRIME array showing difference in resistivity between 6 April 2018 and baseline data acquired on 21 July 2017. (c) Daily temperature and modeled effective rainfall, with the date of the data shown in Figure 6b indicated by a red line. (d) Average resistivity changes with time in the across and upslope lines. LiDAR data used to generate the grayscale topographic base plots in (a) and (b) are provided under the Open Government License (nationalarchives.gov.uk), © Environment Agency.

rates of infiltration. Areas of resistivity increase and decrease are observed in the time-step resistivity models from 6 April 2018 (Figure 6b), which were acquired after a prolonged period of seasonal rainfall over the winter and spring months (Figure 6c). Deeper parts of the PSA show relative decreases in resistivity associated with increased infiltration, whereas no resistivity decreases within the deeper parts of the subsurface are observed outside of the PSA. The impact of seasonal variations in rainfall is best observed in the surficial (top 2 m) layer of the array, which shows increasing and decreasing resistivity in response to periods of drying and wetting, respectively (Figure 6d).

The PSA at Leys Bend has not experienced the loading associated with road construction that is believed to have triggered the two historic landslides; however, changes in climatic patterns may lead to future slope instability due to an infiltration-driven reduction in effective stress. Although the PSA has not displayed any recent displacement that might suggest a change in stress state associated with reactivation, resistivity monitoring allows for tracking of the hydrogeological condition of the PSA. Time-lapse resistivity images of the subsurface therefore contribute to improved understanding of the factors that may act to destabilize this slope in the future.

**Ripley, Canada — Active landslide impacting rail infrastructure.** A PRIME system was used to monitor changes in moisture

content over a two-year period (November 2017–November 2019) on the Ripley landslide, a small, slow-moving, translational landslide in glaciolacustrine clays and Fraser Glaciation lodgement tills in the Thompson River Valley, British Columbia, Canada. The Thompson River Valley is a major transportation corridor that connects Vancouver to the rest of Canada and the United States and is serviced by Canadian Pacific and Canadian National Railway lines. Slope movement associated with the Ripley landslide results in settlement of these railway lines, and failure of the slope could result in blockage of (predominantly freight) trains traveling to and from Vancouver, negatively impacting public safety, the economy, local heritage and communities, and terrestrial and aquatic ecosystems (Huntley et al., 2020).

The PRIME monitoring at the Ripley landslide consists of two linear electrode arrays (2 m spacing between pin electrodes) extending across the head scarp of the landslide (Figure 7a). Measurement sets were acquired automatically once every 12 hours using dipole-dipole configurations. The data were processed and inverted, as detailed in Holmes et al. (2020), and used to better define a 3D ground model of the site.

Resistivity images acquired from the PRIME monitoring were calibrated using petrophysical relationships developed in the laboratory (Holmes et al., 2022a) (Figure 7b). This enabled estimation of moisture content from the resistivity monitoring results

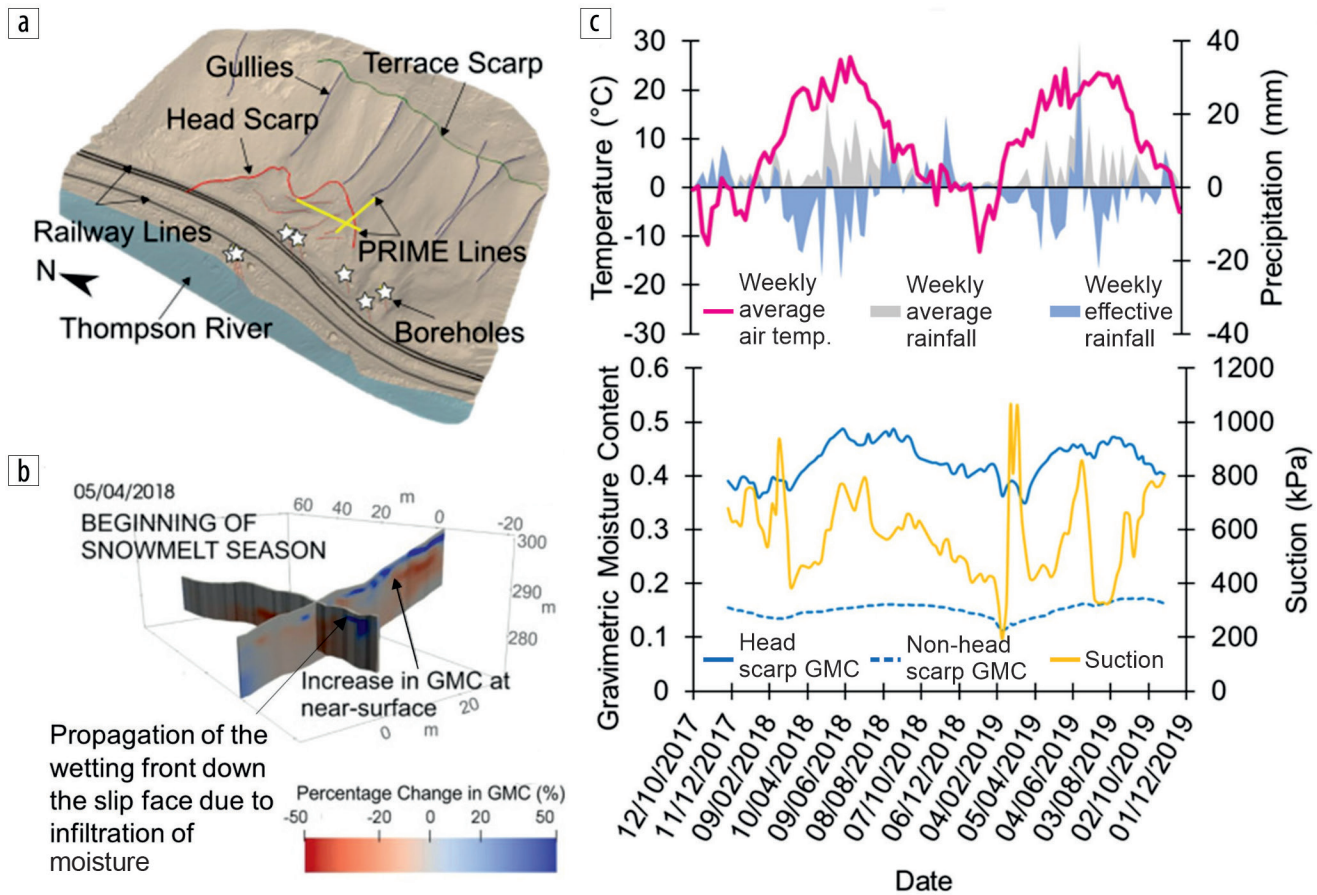


**Figure 7.** (a) Location of PRIME system on the Ripley landslide (after Holmes et al., 2020). (b) Change in GMC from a December baseline image, showing the increase in GMC at the onset of the snowmelt season. (c) Changes in the average resistivity-derived GMC of the head scarp and non-head-scarp zones of the Ripley landslide over the monitoring period, alongside matric suction data for the duration of the study period. Weather data, including air temperature, rainfall, and effective rainfall, are also shown.

so that complex hydrogeological processes could be identified. As shown in Figure 7c, the magnitude of change in GMC over the monitoring period was greater in the head-scarp zone than across the rest of the slope (GMC ranged from 35% to 49% and from 10% to 16% for the head-scarp and non-head-scarp zones, respectively). Additionally, the moisture content of the head-scarp zone remained elevated compared with that of the rest of the PRIME-monitored area of the slope all year round. This is due to tension cracks providing a conduit for infiltration in the head scarp, which in turn can cause a reduction in matric suction and normal effective stress in this zone, increasing the likelihood of failure.

The hydrologic regime of the subsurface and movement of the slope at the Ripley landslide largely depend on seasonal temperature changes (Holmes et al., 2022a), as air temperatures at the site drop below 0°C on an annual basis. Indeed, the greatest changes in GMC at the Ripley landslide occur at the onset of the spring snowmelt season (March–April) when air temperatures rise above 0°C (Figures 7b and 7c). Matric suction decreased around the time of snowmelt following a short period of very high suction due to freezing, as melting of pore fluid occurred, as well as infiltration from the melting snowpack. This has implications for slope stability, as a reduction in suction results in a decrease in shear strength. Further slope movement in the Thompson River Valley, including that of the Ripley landslide, is closely related to the river levels. There was an average of 89.5 mm of downslope

displacement in the main sliding mass over the monitoring period, and the greatest rate of movement occurred between October and April each year. When the Thompson River level is low because of freezing precipitation, this leads to a debutting effect, and when suction levels decrease at the onset of snowmelt, the slope is vulnerable to failure and movement accelerates until the river level rises again in response to snowmelt in the wider Thompson River Valley (Sattler et al., 2021).

## Discussion

The case histories considered here all demonstrate long-term (i.e., multiyear) ERT monitoring of moisture dynamics in highly heterogeneous landslide settings. In all but one case (Ripley), the systems were powered entirely by solar charging of system batteries, and in all cases, data were delivered in near real time via 4G/5G communications, with a temporal frequency of at least several data sets per week — and in some cases several data sets per day. The examples illustrate the flexibility of the monitoring approach with both 2D and 3D imaging arrays and designs tailored to the specific setting.

All of the infrastructure-related examples presented here are in remote or harsh environments, where human access is difficult or undesirable. The option of remote monitoring in these settings is highly beneficial. In the case of UK rail, access is strictly limited for safety reasons. Consequently, the national rail operator is

prioritizing the deployment of remote-condition-monitoring technologies (Network Rail, 2018).

The monitoring has been used to spatially track subsurface processes related to moisture infiltration at the asset or slope scale, encompassing fissured environments, the influence of vegetation on slope hydrodynamics, snowmelt events and drainage, with ERT monitoring results providing direct insights into geotechnical property changes (i.e., moisture content and suction). In doing so, the spatial and volumetric information provided by ERT monitoring contributes highly relevant information to support decision making for the management of unstable slopes.

## Forward look and conclusions

Geoelectrical monitoring is a rapidly developing field with major recent advances in instrumentation, modeling, and the range of applications being considered.

**Instrumentation.** The shift to low-power electronics has driven down ERT instrument costs. This is essential for monitoring scenarios where individual instruments need to be committed for the duration of the monitoring period, which can be many years. With the broader take-up of emerging low-power, low-cost monitoring systems, further economies of scale should be realized in the medium term. Systems also are likely to become more intelligent and integrated, bringing in data from other sensors (e.g., geotechnical/fiber-based sensing) and geophysical monitoring techniques (e.g., passive seismic methods) to trigger and focus measurements, thereby facilitating a shift from automatic to autonomous monitoring.

**Modeling and data processing.** The shift to more intelligent monitoring will also require software developments, such as local (i.e., onboard the instrument) data processing and inversion, and automated interpretation — drawing on techniques from machine learning (i.e., feature tracking and pattern recognition; e.g., Ward et al., 2016). Likewise, integrated monitoring will offer greater opportunities for coupled modeling and interpretation to reduce uncertainties and produce more robust interpretations of imaging results (e.g., Slater and Binley, 2021).

**Applications.** Along with landslide monitoring, the sensitivity of ERT to moisture-driven processes means it is suitable for addressing many other environmental and engineering problems. In particular, PRIME is currently being developed for reservoir and tailings dam monitoring — for which the spatial and temporal resolution and deployment scales are ideally suited. In addition, the technology is being used for hydrogeological studies to track saline intrusion and contaminant transport.

The most effective and appropriate use of ERT monitoring is as a tool within a broader toolbox of techniques including, for example, remote sensing, other geophysical techniques measuring complementary parameters, and intrusive investigations. However, our increasing ability to provide volumetric subsurface information at high spatial and temporal resolution clearly demonstrates the crucial contributions of geophysical monitoring to the field of geohazard monitoring and early warning. ■■

## Acknowledgments

The authors wish to thank Network Rail (UK), National Highways (UK), Canadian National Railway (Canada), and

Canadian Pacific Railway (Canada) for facilitating the research. The paper is published with the permission of the executive director of the British Geological Survey (BGS) (UKRI). The BGS contribution is linked to the PRIME (grant reference NE/P00914X/1) and ACHILLES (grant reference EP/R034575/1) projects.

## Data and materials availability

Data associated with this research contain both available and confidential elements. Available elements can be obtained by contacting the corresponding author.

Corresponding author: jecha@bgs.ac.uk



© 2022 British Geological Survey/UKRI. Published by the Society of Exploration Geophysicists. All article content, except where otherwise noted (including republished material), is licensed under a Creative Commons Attribution 4.0 International License (CC BY) license. See <https://creativecommons.org/licenses/by/4.0/>. Distribution or reproduction of this work in whole or in part commercially or noncommercially requires full attribution of the original publication, including its digital object identifier (DOI).

## References

- Dimech, A., L. Cheng, M. Chouteau, J. Chambers, S. Uhlemann, P. Wilkinson, P. Meldrum, B. Mary, G. Fabien-Ouellet, and A. Isabelle, 2022, A review on applications of time-lapse electrical resistivity tomography over the last 30 years: Perspectives for mining waste monitoring: *Surveys in Geophysics*, <https://doi.org/10.1007/s10712-022-09731-2>.
- Early, K. R., and P. G. Jordan, 1985, Some landslipping encountered during construction of the A40 near Monmouth: *Quarterly Journal of Engineering Geology and Hydrogeology*, **18**, 207–224, <https://doi.org/10.1144/GSL.QJEG.1985.018.03.03>.
- Fan, X., A. Dufresne, J. Whiteley, A. P. Yunus, S. S. Subramanian, C. A. U. Okeke, T. Pánek, et al., 2021, Recent technological and methodological advances for the investigation of landslide dams: *Earth-Science Reviews*, **218**, 103646, <https://doi.org/10.1016/j.earscirev.2021.103646>.
- Gunn, D., B. A. J. Dashwood, P. Bergamo, and S. Donohue, 2016, Aged embankment imaging and assessment using surface waves: *Proceedings of the Institution of Civil Engineers — Forensic Engineering*, **169**, no. 4, 149–165, <https://doi.org/10.1680/jfoen.16.00022>.
- Hobbs, P. R. N., D. C. Entwisle, K. J. Northmore, M. G. Sumblar, L. D. Jones, S. Kemp, S. Self, et al., 2005, The engineering geology of UK rocks and soils: The Lias Group, British Geological Survey Internal Report, IR/05/008.
- Holmes, J., J. Chambers, P. Meldrum, P. Wilkinson, J. Boyd, P. Williamson, D. Huntley, et al., 2020, Four-dimensional electrical resistivity tomography for continuous, near-real time monitoring of a landslide affecting transport infrastructure in British Columbia, Canada: *Near Surface Geophysics*, **18**, no. 4, 337–351, <https://doi.org/10.1002/nsg.12102>.
- Holmes, J., J. Chambers, P. Wilkinson, P. Meldrum, M. Cimpoiaşu, J. Boyd, D. Huntley, et al., 2022a, Application of petrophysical relationships to electrical resistivity models for assessing the stability of a landslide in British Columbia, Canada: *Engineering Geology*, **301**, 106613, <https://doi.org/10.1016/j.enggeo.2022.106613>.

- Holmes, J., J. Chambers, P. Wilkinson, B. Dashwood, D. Gunn, M. Cimpoişu, M. Kirkham, et al., 2022b, 4D electrical resistivity tomography for assessing the influence of vegetation and subsurface moisture on railway cutting condition: *Engineering Geology*, **307**, 106790, <https://doi.org/10.1016/j.enggeo.2022.106790>.
- Huntley, D., J. Holmes, P. Bobrowsky, J. Chambers, P. Meldrum, P. Wilkinson, S. Donohue, et al., 2020, Hydrogeological and geophysical properties of the very-slow-moving Ripley landslide, Thompson River Valley, British Columbia: *Canadian Journal of Earth Sciences*, **57**, no. 12, 1371–1391, <https://doi.org/10.1139/cjes-2019-0187>.
- Intrieri, E., G. Gigli, N. Casagli, and F. Nadim, 2013, Brief communication: Landslide early warning system: Toolbox and general concepts: *Natural Hazards and Earth System Sciences*, **13**, 85–90, <https://doi.org/10.5194/nhess-13-85-2013>.
- Kelevitz, K., A. Novellino, A. Watlet, J. Boyd, J. Whiteley, J. Chambers, C. Jordan, T. Wright, A. Hooper, and J. Biggs, 2022, Ground and satellite-based methods of measuring deformation at a UK landslide observatory: Comparison and integration: *Remote Sensing*, **14**, no. 12, 2836, <https://doi.org/10.3390/rs14122836>.
- Khan, S., J. Ivoke, and M. Nobahar, 2019, Coupled effect of wet-dry cycles and rainfall on highway slope made of Yazoo clay: *Geosciences*, **9**, no. 8, 341, <https://doi.org/10.3390/geosciences9080341>.
- LaBrecque, D. J., G. Heath, R. Sharpe, and R. Versteeg, 2004, Autonomous monitoring of fluid movement using 3-D electrical resistivity tomography: *Journal of Environmental and Engineering Geophysics*, **9**, no. 3, 167–176, <https://doi.org/10.4133/JEEG9.3.167>.
- Lapenna, V., and A. Perrone, 2022, Time-lapse electrical resistivity tomography (TL-ERT) for landslide monitoring: Recent advances and future directions: *Applied Sciences*, **12**, no. 3, 1425, <https://doi.org/10.3390/app12031425>.
- Loke, M. H., T. Dahlin, and D. F. Rucker, 2014, Smoothness-constrained time-lapse inversion of data from 3D resistivity surveys: *Near Surface Geophysics*, **12**, no. 1, 5–24, <https://doi.org/10.3997/1873-0604.2013025>.
- Network Rail, 2018, Earthworks technical strategy, June 2018: Network Rail, UK.
- Sattler, K., D. Elwood, M. T. Hendry, D. Huntley, J. Holmes, P. B. Wilkinson, J. Chambers, et al., 2021, Quantifying the contribution of matric suction on changes in stability and displacement rate of a translational landslide in glaciolacustrine clay: *Landslides*, **18**, 1675–1689, <https://doi.org/10.1007/s10346-020-01611-3>.
- Slater, L., and A. Binley, 2021, Advancing hydrological process understanding from long-term resistivity monitoring systems: *WIREs Water*, **8**, no. 3, e1513, <https://doi.org/10.1002/wat2.1513>.
- Smedley, M. I., R. Paulson, and A. Tucker, 2009, Remote sensing for highway management of landslides: *Proceedings of the Institution of Civil Engineers — Geotechnical Engineering*, **162**, no. 3, 141–150, <https://doi.org/10.1680/geng.2009.162.3.141>.
- Smethurst, J. A., A. Smith, S. Uhlemann, C. Wooff, J. Chambers, P. Hughes, S. Lenart, et al., 2017, Current and future role of instrumentation and monitoring in the performance of transport infrastructure slopes: *Quarterly Journal of Engineering Geology and Hydrogeology*, **50**, no. 3, 271–286, <https://doi.org/10.1144/qjegh2016-080>.
- Tresoldi, G., D. Arosio, A. Hojat, L. Longoni, M. Papini, and L. Zanzi, 2019, Long-term hydrogeophysical monitoring of the internal conditions of river levees: *Engineering Geology*, **259**, 105139, <https://doi.org/10.1016/j.enggeo.2019.05.016>.
- Uhlemann, S., J. Chambers, P. Wilkinson, H. Maurer, A. Merritt, P. Meldrum, O. Kuras, D. Gunn, A. Smith, and T. Dijkstra, 2017, Four-dimensional imaging of moisture dynamics during landslide reactivation: *Journal of Geophysical Research: Earth Surface*, **122**, no. 1, 398–418, <https://doi.org/10.1002/2016JF003983>.
- Versteeg, R., M. Ankeny, J. Harbour, G. Heath, K. Kostelnik, E. Mattson, K. Moor, A. Richardson, and K. Wangerud, 2004, A structured approach to the use of near-surface geophysics in long-term monitoring: *The Leading Edge*, **23**, no. 7, 700–703, <https://doi.org/10.1190/1.1776745>.
- Vivoni, E. R., A. J. Rinehart, L. A. Méndez-Barroso, C. A. Aragón, G. Bisht, M. Bayani Cardenas, E. Engle, et al., 2008, Vegetation controls on soil moisture distribution in the Valles Caldera, New Mexico, during the North American monsoon: *Ecology*, **1**, no. 3, 225–238, <https://doi.org/10.1002/eco.11>.
- Ward, W. O. C., P. B. Wilkinson, J. E. Chambers, H. Nilsson, O. Kuras, and L. Bai, 2016, Tracking tracer motion in a 4-D electrical resistivity tomography experiment: *Water Resources Research*, **52**, no. 5, 4078–4094, <https://doi.org/10.1002/2015WR017958>.
- Wilkinson, P., J. Chambers, S. Uhlemann, P. Meldrum, A. Smith, N. Dixon, and M. H. Loke, 2016, Reconstruction of landslide movements by inversion of 4-D electrical resistivity tomography monitoring data: *Geophysical Research Letters*, **43**, no. 3, 1166–1174, <https://doi.org/10.1002/2015GL067494>.
- Whiteley, J. S., J. E. Chambers, S. Uhlemann, P. B. Wilkinson, and J. M. Kendall, 2019, Geophysical monitoring of moisture-induced landslides: A review: *Reviews of Geophysics*, **57**, no. 1, 106–145, <https://doi.org/10.1029/2018RG000603>.
- Whiteley, J. S., A. Watlet, J. M. Kendall, and J. E. Chambers, 2021, Brief communication: The role of geophysical imaging in local landslide early warning systems: *Natural Hazards and Earth System Sciences*, **21**, no. 12, 3863–3871, <https://doi.org/10.5194/nhess-21-3863-2021>.